Assessment of the Deformation Demand in Multi-Storey Frames

F. Mollaioli, A. Mura, and L.D. Decanini

University of Rome "La Sapienza", Faculty of Architecture "L. Quaroni",
Department of Structural and Geotechnical Engineering, Rome, Italy,
email: fabrizio.mollaioli@uniroma1.it

ABSTRACT: *The characterization of the seismic behaviour of multi-storey structural systems subjected to severe ground motions requires the study of the response at global and local levels. This is because it can be characterized by high demands for inelastic displacement and energy dissipation, often causing concentration of damage in limited zones of the structure, as weak or soft stories. In order to evaluate the seismic demands on multi-degree-of-freedom (MDOF) systems subjected to severe ground motions, a simplified procedure based on an equivalent discrete shear-type model is presented. This choice provides a relatively simple numerical procedure which is adopted permitting (i) to extend the analyses to a wide range of strong motion records and structures, (ii) to establish response spectra of the inter-storey drifts, (iii) to investigate the dependence of the results on variations in stiffness distribution pattern and ductility at global and local levels. Finally, the influence of hysteretic and inelastic behavior at the same levels is also analyzed.*

Keywords: Multi-storey frames; Ground motions; Equivalent discrete shear-type model; Drift demand

1. Introduction

The aim of this paper is to improve the understanding of behaviour patterns of seismic demands on multi-degree-of freedom (*MDOF*) systems, representative of regular frames, subjected to ground motions of different characteristics.

Recent studies on the interpretation of the behaviour of structures during severe earthquakes have suggested the need for formulating new and more complete procedures for the reliable definition of seismic demand. In evaluating the actual earthquake destructiveness, it is necessary to consider both ground motion and structural characteristics [1-12] adequately. In some cases, the global demands on an earthquake-resistant structure can be estimated from the seismic demand obtained in *SDOF* and equivalent *SDOF* (*ESDOF*) systems. In other cases an *SDOF* model cannot be used to estimate the storey and local seismic demands in multi-storey buildings, due to the presence of local effects, such as inter-storey drifts, local rotations, etc. The way these local effects occur depends on the excitation and on the structural characteristics and cannot be predicted by means of *SDOF* and *ESDOF* responses. It would be ideal to perform seismic demand studies on three-dimensional *MDOF* systems, since the dynamic behaviour of real structures depends on many parameters. However, some authors have decided to focus the analyses on simplified *MDOF* models in order to gain insight into basic dynamic behavior patterns, particularly in the inelastic range [13-19].

The evaluation of the demand patterns as a function of the properties of multi-storey frame structures and ground motion is required to perform extensive analytical parameter studies. With the aim of understanding and quantifying seismic demands for a comprehensive range of ground motions and structure characteristics, a simplified discrete shear-type model with lateral stiffness, inertial and strength characteristics approximating those of the corresponding frame structure and varying along the height is adopted in the present context. This simplified model, developed on purpose by the authors of this paper was used to perform step-by-step dynamic analyses. The contribution of all the

vibration modes of the structure can be implicitly considered for the evaluation of the inelastic response, and the distribution of displacement and energy dissipation on the height of the structure can be adequately described. A validation of the results of the dynamic shear-type analyses is made by means of comparisons with the results derived from analyses performed with more complex models. Seismic demands on *MDOF* systems have been examined in terms of inter-storey drifts, displacement and ductility, in the elastic and inelastic range, and at local and global levels for different stiffness distributions over the height.

The main aspects of this paper are as follows:

1. The authors have been able to obtain synthetic information on local seismic demands in terms of spectra of maximum inter-story drift and top displacements.
2. Ground motions with different characteristics in terms of amplitude, duration and frequency content have been selected in order to provide an estimate of the variability that may occur when different time histories are employed to derive response data. Particular attention has been paid to near-fault type excitations.
3. The influence of target ductility levels, stiffness distribution along the height, and hysteretic models for the detection of a limited set of structural characteristics and behaviour patterns, which are necessary for a proper characterization of local and global structural responses of multi-storey buildings, have been shown.

2. Simplified Nonlinear Dynamic Analysis for Multi-Storey Frames: The Equivalent Discrete Shear-Type Model, ESTM

In the context of the present research, an equivalent discrete shear-type model, namely the *ESTM* model, has been developed and adopted for the evaluation of elastic and inelastic responses of multi-storey frame structures. Using a shear-type model allows a relatively simple procedure in the integration of the equations of motion: if a shear deformation is assumed to describe the lateral deflection of the frame structure, only translational degrees of freedom are included in the calculation. This simplification can provide a good approximation of the numerical solution if an equivalent lateral shear stiffness is given to the model [20-21]. Moreover, the shear drifts of the stories of the equivalent system can consider the influence of the flexural deformations of members, although the rotational degrees of freedom do not explicitly appear in the dynamic analysis of the structure. It is necessary, however, to remember that, for tall frames with a large height/horizontal ratio of length and stiff transverses, a global flexural deformation, with axial deformation of external columns, could become quantitatively considerable. If these effects are needed to be counted, a more complex model, including both global shear and flexural deflection, should be considered. The static condensation of the degrees of freedom of an elastic multi-storey frame system is made possible by the irrelevance of rotational inertial contributions of the masses to the seismic response of this kind of structure. Once the condensation is executed, the equations of motion for the *MDOF* system subjected to a ground acceleration history $\ddot{u}_g(t)$ take the form:

$$\tilde{M}\ddot{u}(t)+\tilde{C}\dot{u}(t)+\tilde{K}u(t)=-\tilde{M}\ I\ \ddot{u}_g(t) \qquad (1)$$

where $\tilde{M}, \tilde{C}$ and $\tilde{K}$ are the translational mass matrix, the damping matrix and the elastic condensed stiffness matrix, respectively, I is a unity vector and $u(t)$ is the vector of the lateral displacements of the stories. It is usual to choose the damping matrix $\tilde{C}$ according to Rayleigh's formulation, i.e. through a linear combination of the matrices $\tilde{M}$ and $\tilde{K}$. The relevant *MDOF* model is represented in Figure (1). This choice allows for reasonable damping effects in all significant modes of vibration with a relatively simple computational procedure, e.g. giving the required nominal damping values to the first three modes. The tri-diagonal form assumed by the matrix $\tilde{C}$ contributes to the computational simplification.

The next step is the individuation of an equivalent shear stiffness matrix, K_S, defined as the tri-diagonal

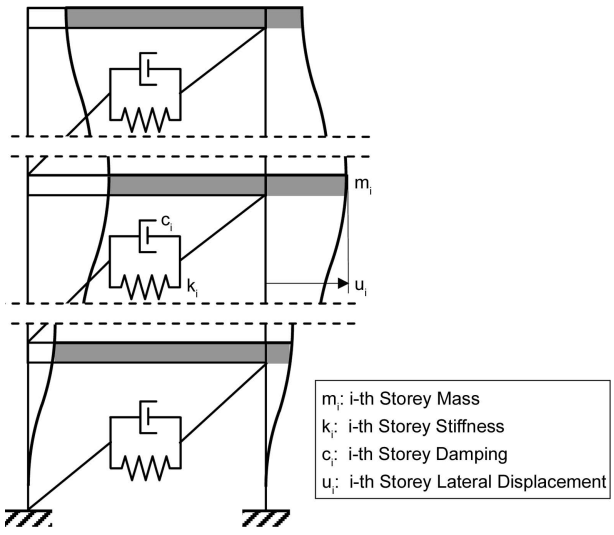

Figure 1. Shear-type *MDOF* model.

stiffness matrix that produces the same lateral displacements related for the stiffness properties of the structure under the action of a prefixed lateral distribution of the static forces. Although this definition is dependent on the distribution of lateral load, differences in the resulting K_S matrix are negligible if reasonable distributions of lateral forces are used. In this study an inverted-triangular static force pattern has been applied. Adopting this procedure, the structural system is completely described by the stiffness and mass properties of the stories. For the prediction of the inelastic response of a frame structure subjected to a ground motion, a stiffness degrading hysteresis model has been defined and developed by the authors in order to describe the cyclic behaviour at each storey level. As for the storey stiffness, also an approximate storey yielding resistance is defined. This approximation implies neglecting some information on local inelastic deformations and hysteretic dissipations, as plastic curvature and dissipated energy in portions of members. The main local displacement parameter directly obtainable by the above described method is the inter-storey drift ratio or index (*IDI*), defined as the inter-storey drift normalized by the storey height, h ($IDI = \delta/h$, where δ is the inter-storey relative displacement). Such an index can provide some indications on the damage at the ends of the columns of each storey, but only presents indirect and rough indications on damage of joints and beams. On the other hand, this simplification allows one to conduct a wide range of investigations into the inelastic seismic response of multi-storey buildings. This is because the resistance properties of the frames can be described by means of a few number of basic parameters and the description of any construction details is not directly required. It is important to note that, in the strength evaluation, a shear-type model cannot consider the effects of the variation of axial forces in the columns.

2.1. Validation of the ESTM Model

In order to evaluate the effectiveness of the proposed simplified methodology, the results computed with the *ESTM* model were compared with those computed with more detailed non-linear time history analyses performed on different framed structures, designed according to different seismic codes. Herein, for the sake of brevity, the results corresponding to two groups of frames will be shown. The first group consists of two-bay frames of six and twelve stories designed in accordance with the requirements for full ductility specified in the New Zealand codes, and studied by Watson [22]. For these ductile frames, the capacity design procedure proposed by Park and Paulay [23] was applied. A two-dimensional inelastic time-history analysis was used to investigate the response of the designed structure, where its structural components were modelled by the use of a one-dimensional prismatic member element with a spring hinge at each end. A bilinear moment-curvature hysteretic model was used for beams and columns. The two-dimensional frames were subjected to three different ground motion records obtained during the 1940 Imperial Valley ($M = 6.4$; El Centro recording station, *NS* component), 1966 Parkfield ($M = 5.6$; Parkfield N.2 recording station, *N*65*E* component), and 1971 San Fernando ($M = 6.4$; Pacoima Dam recording station, *S*14*W* component) earthquakes. In particular, for the twelve storey ductile frame, two records were applied, namely the *El* Centro and Pacoima Dam records, while for the six storey ductile frame, three records were used, namely the El Centro, Parkfield and Pacoima Dam records. In Figure (2), the comparison of maximum inter-storey drift ratios (*IDI*) for the twelve and six storey buildings is shown. Differences in the inter-storey drifts obtained from the results of *ESTM* and Watson [22] analyses depends on the type of the record and do not exceed 25 percent. However, divergences of such magnitude are not observed in stories where the maximum *IDI* demand occurs.

The second group consists of typical symmetric *RC*, two-bay frames of six and twelve stories analysed by Mazza and Vulcano [24] and designed according to *EC*8 [25], assuming enhanced ductility class *DCE*, two subsoil classes *A* and *C*, and high-risk seismic region. The capacity design criterion of *EC*8 [25] is satisfied in all the beam-column joints. The frames were subjected to both artificially generated and recorded time histories. The response spectrum of the simulated accelerograms matches that adopted by *EC*8 for a magnitude $M_S \geq 5.5$ assuming either subsoil class *A* (*EC*8.*A*) or subsoil class *D* (*EC*8.*D*). Moreover, natural near-fault ground motions were selected for the non-linear analyses. In this paper, the comparison is limited to two near-fault motions obtained during the 1992 Landers Earthquake ($M_w = 7.2$; Lucerne recording station, rock-site) and 1992 Cape Mendocino Earthquake ($M_w = 7.0$; Petrolia recording station, soil-site). Figures (3) and (4) show the maximum inter-storey drifts as computed by Mazza and Vulcano [24] and as determined by the

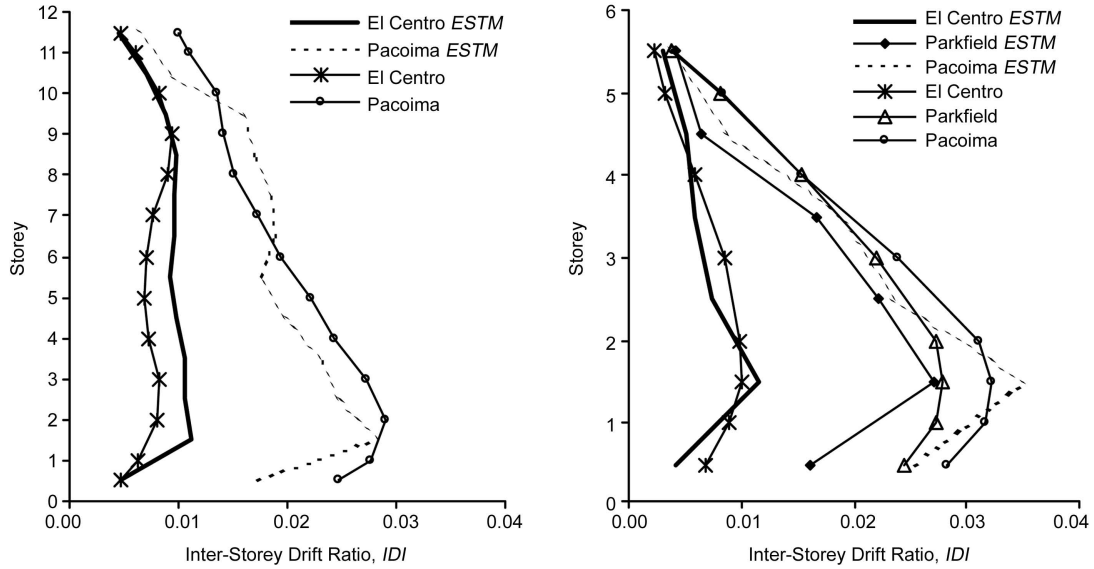

Figure 2. Comparison of inter-storey drift ratios, *IDI*. *ESTM* vs. Watson [22] results. 12 and 6 storey frames.

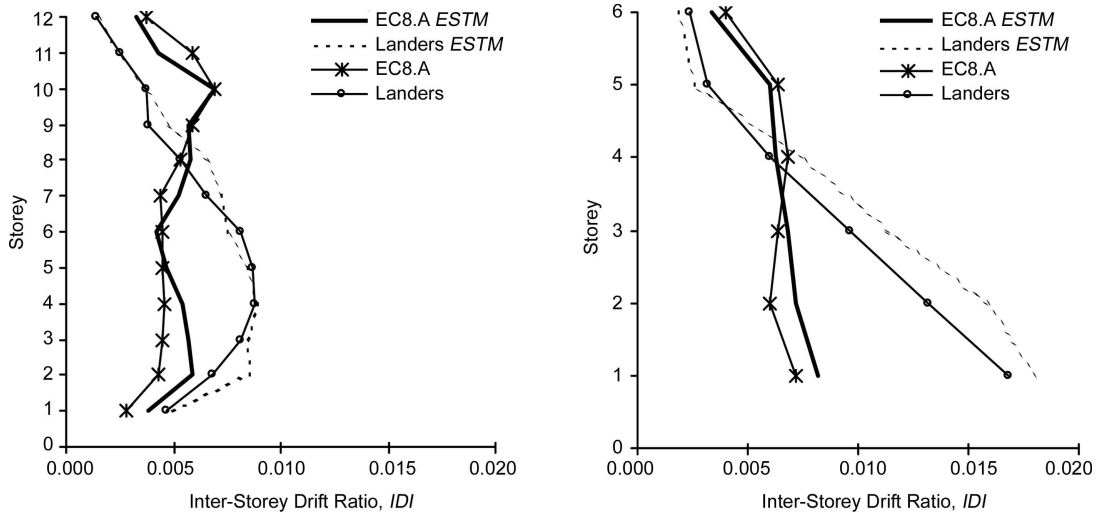

Figure 3. Comparison of inter-storey drift ratios, *IDI*. *ESTM* vs. Mazza and Vulcano [24] results. 12 and 6 storey frames. Stiff soils.

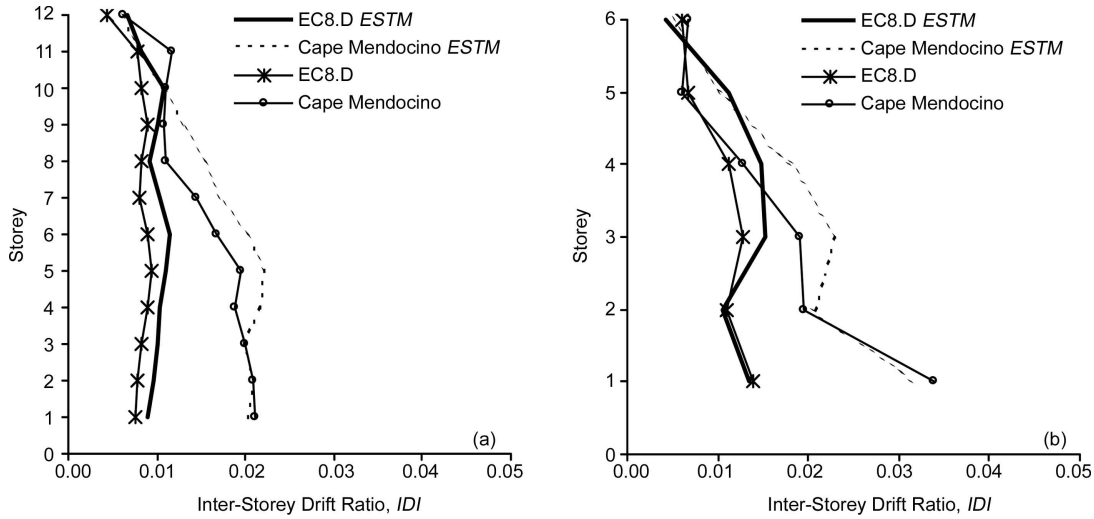

Figure 4. Comparison of inter-storey drift ratios, *IDI*. *ESTM* vs. Mazza and Vulcano [24] results. 12 and 6 storey frames. Soft soils.

ESTM analyses for *EC*8. *A* and Landers records and for *EC.D* and Cape Mendocino records, respectively. In this case the *ESTM* analysis seems to slightly overestimate the exact results, with an increasing trend in the difference going from firm to soft soils.

However, the storey where the maximum drift occurs is the same for both types of analyses. In conclusion, it is possible to assert that: (1) the outline along the height of the drift demand presents an almost similar shape for all types of analyses; (2) in each of the cases shown, the inter-storey drift is fairly well represented by the *ESTM* results; and (3) the discrepancies between *ESTM* and exact results tend to increase as the soil stiffness decreases. The fact that the *ESTM* method allows to estimate the response of framed structures to a similar degree of accuracy of a more detailed dynamic analyses indicates that this procedure is accurate enough for the assessment of the seismic demand for the *MDOF* systems examined. This applies particularly when the seismic demand itself is characterized by the maximum inter-storey drift ratio.

3. Structural Systems and Ground Motions

The availability of an adequate simplified model, capable of giving a fairly accurate estimate of the seismic response of *MDOF* systems at global and local levels, permits to obtain a spectral representation of the most significant seismic demand parameters and to perform broad parametric analyses on different structures. In this research, ten multi-storey structural systems, having ten different number of stories (N = 2, 4, 6, 8, 10, 12, 14, 16, 20, 24) modelled by using two-dimensional, two-bay generic frames with constant storey height ($h = 3.2m$) and beam spans ($w = 5.0m$), were studied in order to capture the influence of some of the significant structural parameters, and to obtain information on the seismic response of a wide range of current buildings.

It seems worthwhile to assess if the number of bays is significant in representing the performance of multi-bay frames. The comparisons of the responses of frames having different number of bays (from one to four bays) showed that the responses are very similar in terms of displacement and energy demands [21, 26, 27, 28]. Therefore, two-bay standard frames can generally be considered adequate to describe the global behaviour of a regular multi-bay frame.

For each selected frame, three different stiffness patterns have been assumed: (1) a realistic, approximately parabolic stiffness distribution with full constraint for the joints at the base of the columns (stiff soil-foundation structures), (pattern *a*); (2) the same stiffness distribution as pattern "*a*", with some degree of flexibility of the soil-foundation system, (pattern *b*); (3) a uniform distribution of stiffness along the height, calibrated so as to obtain the same vibration periods of the stiffness distribution "*a*" (pattern *u*). In Table (1), the first periods of vibration for frames with different number of stories are provided. The periods have been calculated in the elastic range of behaviour, considering cracked elements. To account for pre-yield cracking, 50% of the gross section stiffness (EI_g) for beams, 90% EI_g for interior columns and 70% EI_g for exterior columns have been used.

Table 1. First periods of vibration of the analyzed *R/C* frames.

N	T_1 (s)	
	Patterns *a* and *u*	Pattern *b*
2	0.28	0.34
4	0.54	0.58
6	0.76	0.81
8	1.02	1.06
10	1.25	1.30
12	1.47	1.51
14	1.66	1.70
16	1.87	1.91
20	2.34	2.37
24	2.69	2.72

The base resistance has been derived from linear and nonlinear analyses executed on *SDOF* systems, with periods equal to the fundamental periods of the frames and for defined values of target ductility (μ = 1.5, 2, 4 and 6). After calculating the seismic coefficient C_y that leads the *SDOF* system to the target ductility value, the yielding shear at the base of the structure is evaluated as

$$V_{by} = M_{tot} C_y g \tag{2}$$

assuming the total mass M_{tot} of the frame as a global "effective" mass, that is attributed to the first mode of vibration. One could assume the real effective mass of some modes of vibration and combine the modal values of C_y, but preliminary analyses have shown that no improvement would be obtained in terms of precision in reaching the assigned target ductility. The yielding strengths of the stories have been obtained by an inverted-triangular distribution of equivalent seismic forces, with an additional force

at the top of the building with fundamental periods longer than 0.7*s*. In the adopted simplified modelling, it was necessary to manage the local inelastic behaviour adequately which operates at storey level in the *ESTM* model, in order to obtain a well-designed frame where the so-called beam-sway mechanism is ensured. This implies that plastic hinges are formed in all beams at all storeys, while the strength capacity of columns and joints is preserved. By means of comparison with other researches [2, 29] and *ad hoc* analyses, the strain hardening of the considered hysteretic model was identified as a simple tool capable to ensure a beam-sway mechanism. Such assertion is based prevalently on the fact that the stiffness reduction caused by the concentration of plastic deformations in the beams of a given storey, though significant, is less rapid than in occurrence of a storey mechanism. For this reason, the strain hardening ratio, p, was tuned to a value $p = 0.1$ for properly designed *RC* frames. Rayleigh damping has been used to obtain a 5% of critical damping in the first and third mode.

A stiffness-degrading hysteretic model was adopted for the cyclic behaviour of the frames in each storey. The hysteresis model is developed and used in this study. Figure (5) utilises several control parameters that establish the rules for inelastic loading reversals. It is based on the hysteresis model proposed by Kunnath et al [30] and modified by substituting $u_{ult,\ mon}$ (monotonic ultimate displacement) with u_y (yielding displacement), for the purpose of performing analyses at constant target ductility ratios.

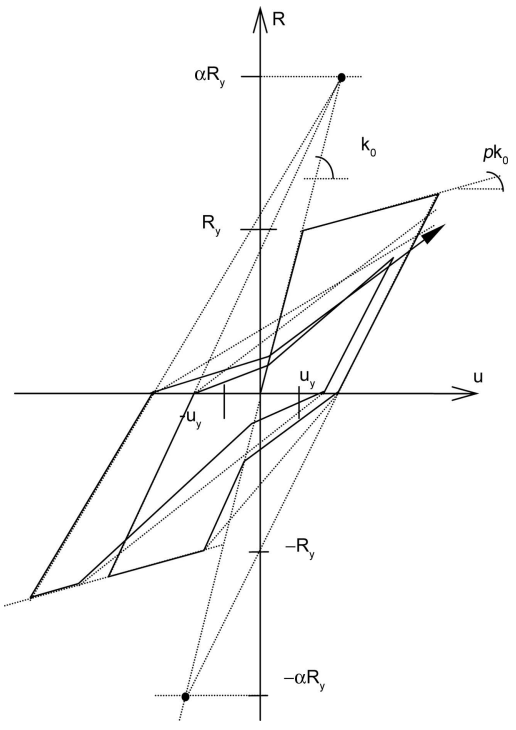

Figure 5. Typical cyclic behaviour of the four parameter hysteretic model used in this study.

The constitutive law is governed by four parameters, namely p, α, β, γ. The parameter p, the strain hardening ratio introduced above, controls the post-yielding stiffness and is set equal to 0.1; α is related to the unloading stiffness; β controls the strength degradation; and γ controls the pinching effect due to closing cracks during the reloading phase. If α tends to infinity, there is no stiffness degradation during the unloading phase; and the value $\alpha = 2$ represents a mean value. For $\beta = 0$, there is no strength degradation due to energy dissipation; the value $\beta = 0.1$ corresponds to a mean value for which this effect is quite reasonable and for larger values it can lead to unrealistic results or produce numerical instability. For $\gamma = 1$, there is no pinching, while $\gamma = 0$ corresponds to the maximum pinching effect and; $\gamma = 0.5$ can be considered a realistic value.

The force-deformation behaviour in concrete structures is influenced by many factors such as the nature of the response and the level of the reinforcement detailing. In such cases, it is necessary to include more than one type of degrading behaviour to model the expected response.

Two extreme patterns of behaviour can be considered:

- Stable flexural response (characteristic of well-detailed, well-confined flexural elements);
- Severely degraded response (likely to be observed in critical elements, whose behaviour is governed by shear failure, such as inadequately reinforced concrete joints and bad detailed short columns or coupling beams).

Thus, on the basis of the aforementioned consideration, six histeretic models were selected:

- The elastic-perfectly plastic model, *EPP*, introduced as a term of comparison; and five degrading models:
- *DGR*1 (with reloading stiffness degradation and no strain hardening);
- *DGR*2 (with reloading stiffness degradation and strain hardening ratio $p = 0.1$);
- *DGR*3 (with reloading and unloading stiffness degradation and strain hardening ratio $p = 0.1$);
- *DGR*4 (with reloading and unloading stiffness degradation, pinching effect and strain hardening ratio $p = 0.1$);
- *DGR*5 (with reloading and unloading stiffness degradation, strength deterioration and strain hardening ratio $p = 0.1$).

It is also possible to note that, unless secondary

effects on more internal cycles are considered, the *DGR*1 and *DGR*2 models correspond to the Clough model [31] without and with strain hardening, respectively, while the DGR3 model matches the Takeda model [32].

3.1. Ground Motion Selection

The choice of a data-set of accelerograms adequate to represent the significant characteristics of the seismic demand on the analyzed structures, is a fundamental step. The selection has involved only natural signals, with a relevant damage potential demand both in terms of displacements and energy dissipation. The analysis of the structural behaviour observed during recent earthquakes has shown the importance of pulses, especially for near-fault records. For this reason, a large number of near-fault signals have been included in the data-set, by considering both forward and backward directivity effects. By means of preliminary analyses on *SDOF* systems, 44 records were finally chosen to account for different seismic conditions in terms of magnitude (M_w), source-to-site distance (D_f), fault mechanism, and all factors that influence the signal nature.

The selected records have the following features: 1) Most of the records were taken in the near-fault region (distance from the surface projection of the causative fault $D_f \leq 5km$), typically characterized by long duration pulses; 2) Magnitude *M* ranges between 5.8 and 7.9; 3) the ground motions were recorded on different types of soil; 4) Peak Ground Acceleration (*PGA*) lies between 0.16*g* and 1.1*g*; 5) Peak Ground Velocity (*PGV*) is between 18*cm/s* and 176 *cm/s*; 6) Incremental Velocity (*IV*) is between 29 *cm/s* and 285*cm/s*, the largest values corresponding to the near-fault records; and 7) Housner intensity [33] for 5% damping ratio remains between 28*cm* and 587*cm*. In Table (2), the earthquakes from which the time histories were selected, are listed. In Figure (6), the distribution of the records according to magnitude (M_w) and the closest distance from the surface projection of the fault rupture (D_f) is shown. It is possible to note that the records correspond to a wide range of ground motions in order to allow an in-depth investigation on the influence of their characteristics on the variation of the structural properties.

Table 2. Earthquakes and ground motions considered.

Earthquake	Year	M	Recording Station	Earthquake	Year	M	Recording Station
Imperial Valley	1940	7.0	El Centro Array #9	Loma Prieta	1989	6.9	Capitola
Tokachi-Oki	1968	7.9	Hachinoe NS	Landers	1992	7.3	Lucerne #
Tokachi-Oki	1968	7.9	Hachinoe EW	Landers	1992	7.3	Joshua Tree #
Friuli	1976	6.5	Tolmezzo	Erzican	1992	6.7	Erzincan
Romania	1977	7.5	Bucharest-BRI	Northridge	1994	6.7	Rinaldi Receiving Sta #
Tabas	1978	7.4	Tabas	Northridge	1994	6.7	Sylmar - Olive View FF
Montenegro	1979	6.9	Bar-Skupstina Opstine	Northridge	1994	6.7	Newhall - Fire Sta.
Montenegro	1979	6.9	Petrovac-Hotel Oliva	Northridge	1994	6.7	Santa Monica City Hall
Montenegro	1979	6.9	Ulcinj-Hotel Olimpic	Kobe	1995	6.9	Kobe University
Imperial Valley	1979	6.5	El Centro Array #7	Kobe	1995	6.9	KJMA
Imperial Valley	1979	6.5	Agrarias	Kobe	1995	6.9	Takatori
Imperial Valley	1979	6.5	Bonds Corner	Kobe	1995	6.9	Port Island (0 m)
Imperial Valley	1979	6.5	Calexico Fire Station	Dinar	1995	6.4	Dinar
Imperial Valley	1979	6.5	EC Meloland Overpass FF	Kocaeli	1999	7.4	Sakarya
Imperial Valley	1979	6.5	El Centro Array #6	Kocaeli	1999	7.4	Yarimca
Irpinia	1980	6.8	Calitri	Kocaeli	1999	7.4	Duzce-Met.
Cile	1985	7.8	Llolleo	Duzce	1999	7.1	Duzce-Met.
Nahanni	1985	6.8	Site 1	Duzce	1999	7.1	Bolu
San Salvador	1986	5.8	Geotech Investig Center	ChiChi	1999	7.6	TCU129
Superstition Hills	1987	6.5	Parachute Test site	ChiChi	1999	7.6	TCU052
Loma Prieta	1989	6.9	Los Gatos Pres. Center	ChiChi	1999	7.6	TCU068
Loma Prieta	1989	6.9	Corralitos	ChiChi	1999	7.6	TCU065

4. Influence of the Ductility on Maximum Inter-Storey Drift Demand

One of the engineering demand parameters of primary interest for building structures is the maximum storey drift demand, as it may significantly affect the performance of structural, non-structural, and content systems. Such deformation demands are usually

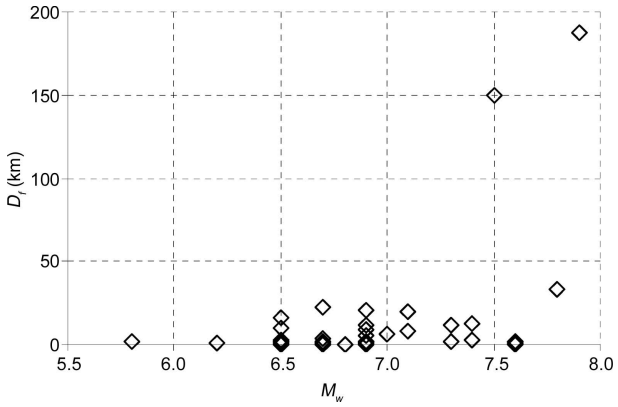

Figure 6. Magnitude versus minimum distance to the causative fault.

characterized through the inter-storey drift index demand, *IDI*. Particularly, the level of damage is always associated with the maximum inter-storey drift demand, IDI_{max}. The elastic and inelastic maximum drift demands are related to the maximum top displacement and significantly influenced by the deformation demand distribution along the height of the building that simultaneously depend on both the earthquake ground motion and the structural characteristics. The maximum top displacement can be approximately estimated by means of equivalent single-degree-of-freedom systems (*ESDOF*), taking into account the contribution of only the first vibration mode of the structure. On the contrary, the local drift demands, at each storey level, can be strongly influenced by the participation of higher vibration modes.

From the analyses carried out with the *ESTM* model, it is possible to observe that the ductility ratio influences the maximum inter-storey drift demand significantly. In Figures (7) and (8), the spectra of the median and median plus standard deviation (median +*SD*) of the ratio between the inelastic and elastic maximum drift indexes ($IDI_{max\mu}$ /$IDI_{max,e}$) for the 44 ground motion records are illustrated on the basis of the stiffness distribution *"a"* and the *DGR*3 hysteretic model. The ratio $IDI_{max\mu}$ /$IDI_{max,e}$ holds the same conceptual meaning of the ratio *R* between the inelastic and the elastic displacement of *SDOF* systems. Generally, with respect to the elastic *IDI*, the inelastic inter-storey drift index shows on average an amplification in the short-period range, similarly to the displacement demands for *SDOF* systems, with a decreasing trend as the fundamental period of the frame increases. As expected, the amplification of the inelastic *IDI* increases significantly with the increase of the ductility ratio. It was also observed that there are slight differences between the inter-storey drift spectra of near-field and far-field records.

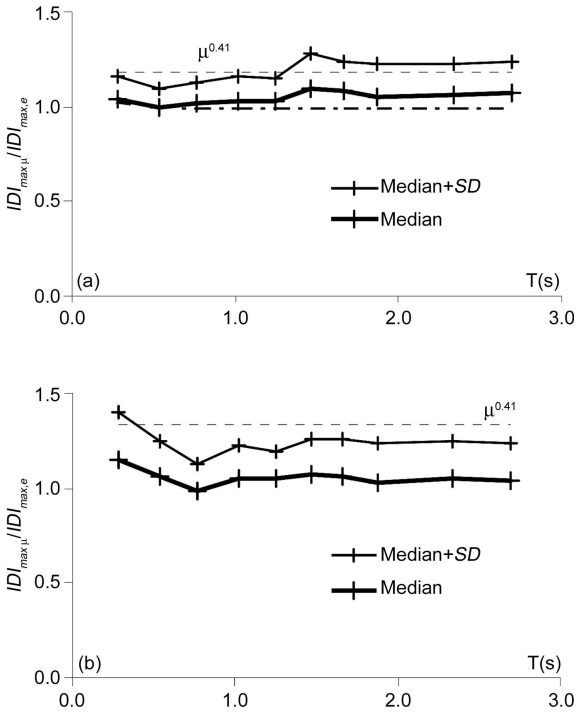

Figure 7. Inelastic to elastic maximum inter-storey drift ratio ($IDI_{max\mu}$ /$IDI_{max,e}$) spectra. Median and median +*SD* (44 strong motion records). Stiffness distribution *a*. *DGR*3 hysteretic model. (a) μ =1.5; (b) μ = 2.

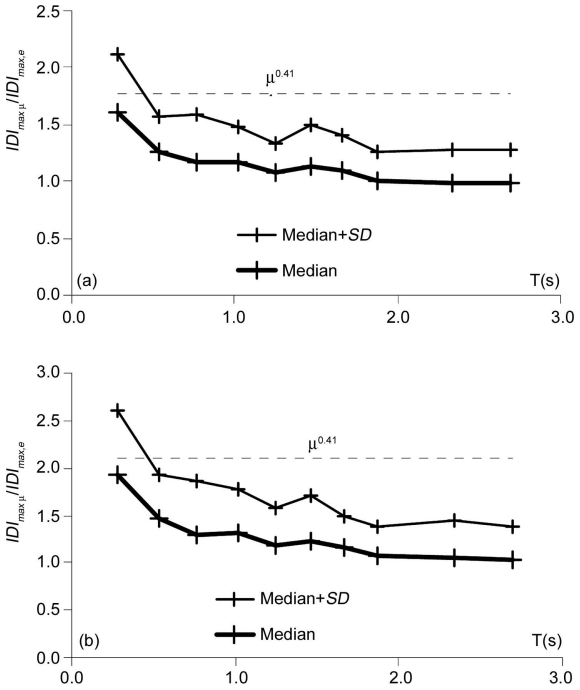

Figure 8. Inelastic to elastic maximum inter-storey drift ratio ($IDI_{max\mu}$ /$IDI_{max,e}$) spectra. Median e median +*SD* (44 strong motion records). Stiffness distribution *a*. *DGR*3 hysteretic model. (a) μ = 4; (b) μ = 6.

The results derived from the *ESTM* model were also compared with the Hwang and Jaw [34] proposal, that provides for the inelastic drift an amplification independent from the vibration period and equal to $\mu^{0.414}$. As shown in Figure (7a), in the low-ductility range (μ =1.5), the median +SD spectrum is approximately in agreement with the Hwang and Jaw's proposal [34], being the inelastic to elastic inter-storey drift ratio not much influenced by the period. It seems reasonable to assume that by considering less flexible frames, the drift amplification could be also higher, for low ductility ratios. For ductilities 2, 4 and 6; see Figures (7b) and (8), the $IDI_{max,\mu}/IDI_{max,e}$ ratio is higher in the short-period range, and in the medium-high period range the Hwang and Jaw's proposal [34] seems to be too conservative. However, for all ductility ratios, the inelastic to elastic inter-storey drift ratio tends, on average, to be 1 for $T \geq 2\text{-}2.5s$.

Another important issue that should be addressed is constituted by the characterization in spectral terms of the storey level where the inelastic drift demand attains its maximum value. In the elastic range, this level is determined as a function of the stiffness distribution pattern and the frequency content of ground motion from which depends the excitation of the structural vibration modes. For frames with stiffness decreasing from the bottom upwards, such as the stiffness scheme *a*, the maximum elastic drifts tend to converge to one of the levels above the first storey. In Figure (9), where the relative height of occurrence of the maximum drift, n_{IDImax}/H, is shown, it is possible to note that the maximum drift is approximately attained at the mid-height of the structure. In the low ductility range ($\mu \leq 2$), the contribution of the higher vibration modes is similar to that obtained in the elastic range, and the drift distribution along the height does not diverge significantly from the elastic one. For larger ductility ratios ($\mu \geq 4$), on average the maximum drift is attained in the lower stories of the structure. This trend (moving of the maximum drift to the lower stories as the ductility ratios increase) is due to the fact that the yielding of a level reduces the propagation of the motion toward the upper levels. Referring to continuum models, such as a shear-beam model [27], this phenomenon can be interpreted as a local decrease of the velocity of seismic waves along the height of the structures, with a consequent concentration of energy dissipation and inelastic deformation.

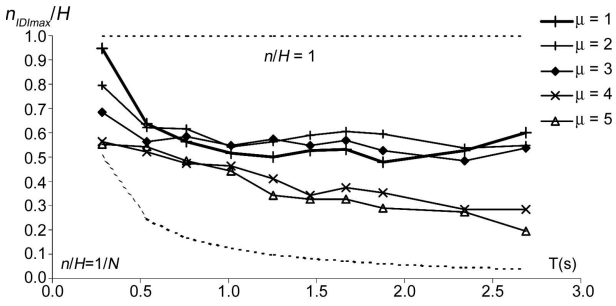

Figure 9. Relative height of occurrence of maximum drift as a function of global ductility ratio. Median values of the response to 44 strong motion records. Stiffness distribution scheme *a*. *DGR*3 hysteretic model.

5. Influence of the Stiffness Distribution Pattern on the Deformation Demand

Another important issue is constituted by the comparison between drift demands obtained for different stiffness distributions through the height of the multi-storey frames. In fact, the adopted stiffness distribution pattern may have influence on the maximum drift values. Generally, the behaviour shown by the scheme *"b"* differs from that of the scheme *"a"* only in the short-period range, due to the influence of the stiffness reduction at the first storey. The uniform stiffness frames (scheme *u*), that are more flexible, are subjected to larger drift demands.

The spectral values of top displacement have not proved to be strongly influenced by the particular stiffness distribution (schemes *a*, *b*, *u*) while differences in the drift demand reach on average almost 30%. This fact can be partially explained with the coincidence of the first vibration periods for the three classes of frames: the top displacement is influenced strongly by the first mode, while the local deformations are often mainly due to higher modes. However, it should be noted that the second and third periods for the three stiffness patterns do not differ greatly. This means that the observed differences of inter-storey drift are caused mainly by the influence of the "modal" inelastic deflection shapes, which are significantly correlated with the stiffness distribution. Such an effect is confirmed by the fact that the elastic spectra show a good coincidence, with the exception of the long-period range, where top displacements also differ.

The stiffness distribution "*u*" significantly influences (for ductility $\mu \geq 4$) the inelastic drift values. The above described trend could be interpreted as a greater tendency for the uniform stiffness pattern to amplify the effects of inelastic behaviour. For a large part of the analysed records, it is evident that, while

in drift spectra the increase of ductility amplifies, the differences between the two stiffness patterns (*a* and *u*), in top displacement spectra decrease from the elastic or low ductility to high ductility ratios.

It is interesting to investigate the inelastic drift amplification analogously to the studies developed for *SDOF* displacement inelastic amplification [11]. Hence the ratio between maximum inelastic inter-storey drift and the corresponding maximum elastic value can be considered. In Figure (10), the median spectra of these ratios are illustrated. Although the ground motions utilized in this study differ noticeably in terms of frequency content, duration and amplitude, it was possible to make some consideration on statistical grounds. First of all, it was noted that for the stiffness distribution pattern "*a*" the mean value of the coefficient of variation, *COV*, of the $IDI_{max\ \mu}/IDI_{max,e}$ parameter ranges between 0.13 and 0.35 for ductility ratios ranging from 1.5 to 6, considering the whole dataset of records. The dispersion tends to slightly increase for the stiffness distribution patterns "*b*" and "*u*". Further comparisons realized by considering the ground motion records enclosed in narrower magnitude and distance bins do not modify substantially the observed trend of the median spectra corresponding to all records.

The stiffness pattern "*a*" shows a general trend very similar to that observed in the traditional inelastic amplification displacement ratios, with high values at short periods, a strong reduction in the medium periods range and an asymptotic convergence to unity for periods longer than 1.25*s*. A less clear trend is shown by the stiffness pattern "*u*". After a similar first decreasing branch, the mean ratios maintain values over 1.2-1.5 also for long periods. A generally more accentuated inelastic amplification trend is confirmed in the uniform stiffness pattern.

In order to better quantify the influence of stiffness distribution on global displacement and maximum drift demand, the ratios between "*u*" and "*a*" results have been calculated. The median values are shown in Figure (11). Considering this aspect not only allows one to understand the stiffness influence on actual structures, but also provides a test of the reliability of uniform equivalent models having the same fundamental periods and the same height as the actual buildings. The results confirm that the stiffness distribution affects the drift demand more than the top displacement. The drift demand is acceptably close for the two patterns, "*a*" and "*u*", in the elastic range, while the results diverge considerably in the inelastic range, with a scarce dependence on the target ductility level. The uniform stiffness distribution confirms to be incorrect for seismic design and inappropriate in evaluating the inelastic drift demand for actual frames.

The maximum inter-storey drift (IDI_{max}) can be related to the average drift (IDI_{avg}) along the height *H* of the frame by means of the coefficient of distortion *COD* [6],

$$COD = IDI_{max}/IDI_{avg} = IDI_{max} \cdot H/d_{top} \tag{3}$$

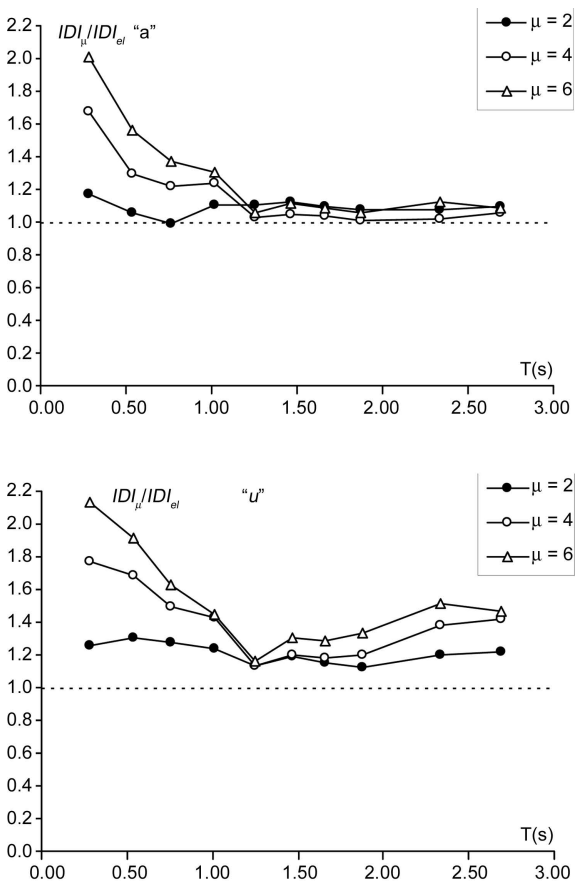

Figure 10. Drift inelastic modification ratios. *DGR*3 hysteretic model. Stiffness patterns *a* and *u*.

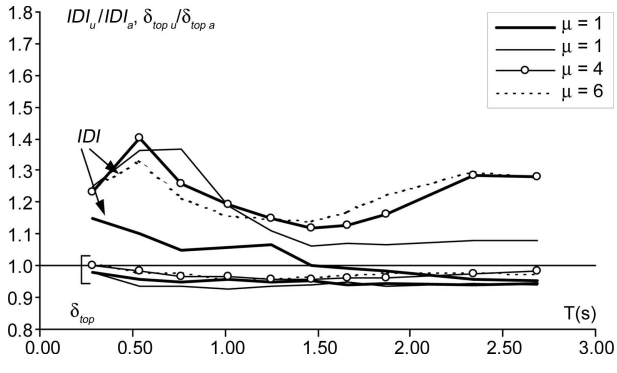

Figure 11. Median values of ratios between *u* and *a* drift and top displacement demands. *DGR*3 hysteretic model.

This coefficient, in the case of regular frames and in the elastic range, gives a measure of the influence of higher modes on the local relative distortions. In the inelastic range, it also furnishes information on the concentration of deformation at the various storeys, and generally tends to increase as the ductility ratio increases. In Figure (12), a comparison between median +*SD* spectra corresponding to the whole database, near-fault (*NF*) and far-field (*FF*) records of the elastic and inelastic coefficient of distortion *COD*, is shown. The coefficient of distortion increases on average with increasing periods. In the elastic range, this is principally due to the effect that higher vibration modes have on tall frames. As already underlined, in the inelastic range, the *COD* tends to increase as the ductility ratio increases, since it is affected by local concentration of inelastic deformation.

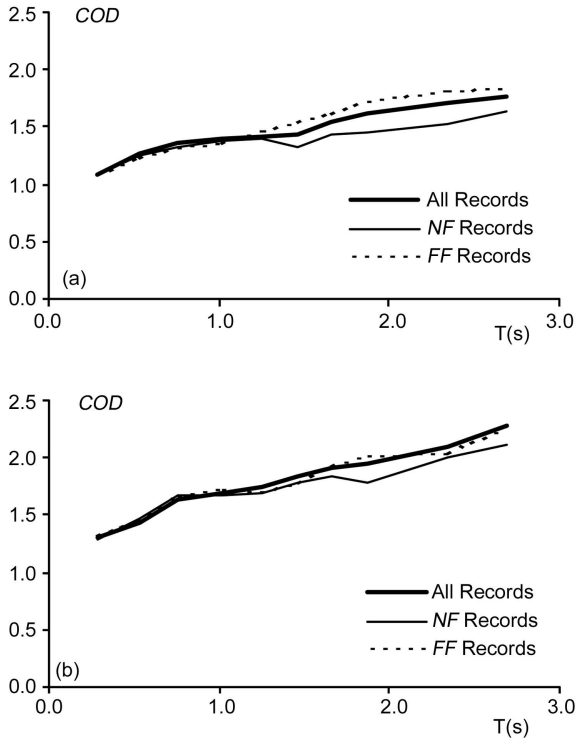

Figure 12. Elastic and inelastic coefficient of distorsion *COD* spectra. Stiffness patterns *a*. Median +*SD* on 44 records. Comparison between global, near-fault (*NF*) and far-field (*FF*) median spectra. Stiffness distribution *a*. *DGR*3 hysteretic model. a) Elastic; b) Inelastic, μ =4.

Figure (13) shows the comparison between a proposal of a design COD_d, corresponding to μ =2.4, evaluated for stiffness distribution patterns "*a*" and "*b*" and on the basis of the median plus one standard deviation of the drift values derived from the considered 44 time histories.

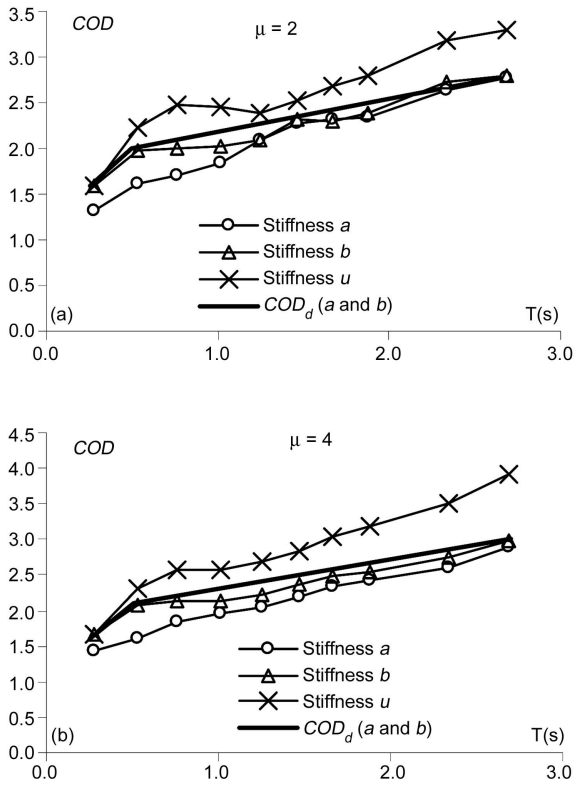

Figure 13. Inelastic coefficient of distorsion. Median +*SD* on 44 records. Comparison between different stiffness patterns and a proposal of a design COD_d for stiffness patterns *a* and *b*. (a) μ =2; (b) μ =4.

In Table (3), the values of the COD_d are reported. In the elastic range, a linear relationship was chosen as suggested by the observed trend of the *COD* spectra. In the inelastic range the proposed relation is bilinear. This proposal has the purpose to suggest reliable values of the *CODs* necessary in the preliminary design, in order to evaluate the maximum inter-storey drift demand to be compared iteratively with the maximum drift supplied by the structure. For example, the prediction of the inter-storey drift can be achieved by means of the equivalent single-degree-of-freedom (*ESDOF*) method. This gives a reliable estimation of the top displacement of the frame, once the inelastic displacement spectrum $\delta_\mu(T)$, obtained from *SDOF* systems for the considered design seismic action and the target ductility ratio μ, is available. The fundamental period *T* could be evaluated in a first phase on the basis of empirical formulae

Table 3. Elastic ($\mu = 1$) and inelastic ($\mu = 2$, $\mu = 4$) design coefficient of distortion (COD_d) values. Regular frames, stiffness distribution patterns *a* and *b*.

T (s)	Elastic	$\mu = 2$	$\mu = 4$
0.25	1.3	1.6	1.6
0.50	-	2.0	2.1
2.70	2.5	2.8	3.0

available in literature. Thus, top displacement can be estimated by the following relationships:

$$\delta_{top} = G_{eq} \cdot \delta_{\mu}(T) \tag{4}$$

where G_{eq} is the participation factor associated to the prevalent deformation selected for the characterization of the *ESDOF* system. For regular frames, such deformation could be chosen linearly variable with the height or coincident with that corresponding to the first vibration mode of the structure. Table (4) reports the values of the participation coefficient corresponding to the first vibration mode of the analyzed frames, as a function of the different stiffness distribution patterns and the number of storeys *N*.

Table 4. Participation factors corresponding to the first vibration mode. Stiffness patterns *a*, *b* and *u*.

N	*a*	*b*	*u*
2	1.21	1.17	1.17
4	1.29	1.28	1.24
6	1.32	1.31	1.26
8	1.32	1.32	1.26
10	1.32	1.32	1.27
12	1.33	1.32	1.27
≥ 14	1.33	1.33	1.27

Finally, from the design spectrum of the coefficient of distortion, COD_d, it is possible to obtain an estimation of the expected maximum inter-storey drift:

$$IDI_{max} = COD_d(T) \cdot \delta_{top} = COD_d(T) \cdot G_{eq} \cdot \delta_{\mu}(T) \tag{5}$$

6. Influence of the Hysteretic Model on the Displacement Demand

As already underlined, the choice of a given type of hysteretic behaviour in the *ESTM* model allows to estimate approximately the degree of local inelastic deformation demand and to provide insight into the global potential plastic mechanism that can develop during cyclic loading in actual structures. Moreover, structural characteristics such as deterioration in strength and degradation in stiffness may significantly affect the response to ground motion.

A first comparison between the selected hysteretic models highlights that the absence of strain hardening causes a significant local concentration of drift and ductility demands in the *ESTM* model that can lead to the formation of a soft-storey mechanism. This phenomenon is detectable in both the *EPP* and *DGR*1 hysteretic models, which present the maximum divergence from the behaviour of other models with strain hardening. Figures (14) and (15) illustrate the effect of the hysteretic behaviour on the maximum ductility demand (μ_{max}) for two different strong motion records, Hachinoe (Tokachi-Oki, 1968) and Takatori (Kobe, 1995) respectively, and two levels of target ductility, $\mu_{target} = 2$ and $\mu_{target} = 6$. As it can be seen, the ductility demand is appreciably larger than the target ductility, particularly for $\mu_{target} = 6$, in the case of the *EPP* and *DGR*1 model. Furthermore, it should also be noted that Hachinoe is a long duration record characterized by several cycles of similar amplitude, while Takatori represents a typical near-fault record.

As already suggested by Nassar and Krawinkler [2], it is not surprising that there is a considerable difference between maximum storey ductility and target ductility, as the local ductility demand is strongly influenced by the mechanism of development of inelastic behaviour. In fact, the amplification of ductility demands increases when storey mechanisms are allowed. Such behaviour occurs when in actual structures there is a formation of plastic hinges in the columns. In the *ESTM* model, the adoption of a strain hardening equal to 10% decreases the storey

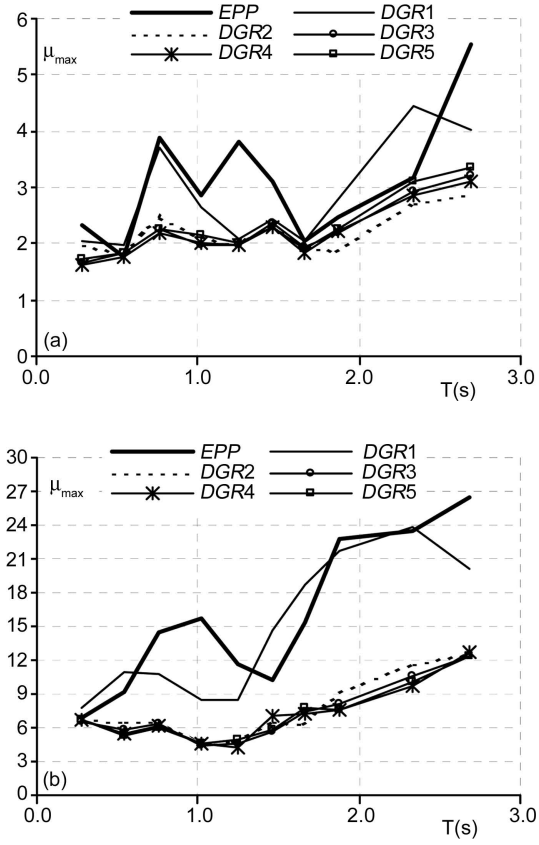

Figure 14. Maximum ductility demand, μ_{max}, spectra. Hachinoe EW record (a) $\mu_{target} = 2$; (b) $\mu_{target} = 6$.

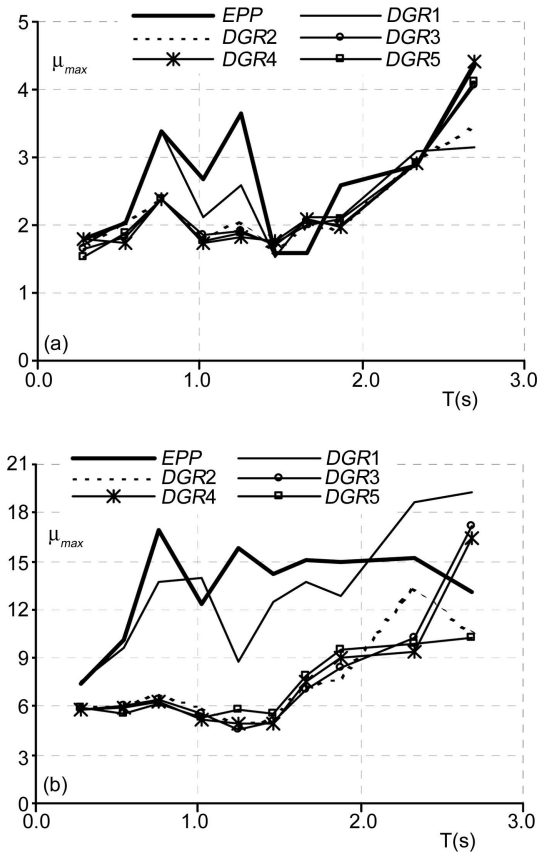

Figure 15. Maximum ductility demand, μ_{max}, spectra. Takatori record (a) $\mu_{target} = 2$; (b) $\mu_{target} = 6$.

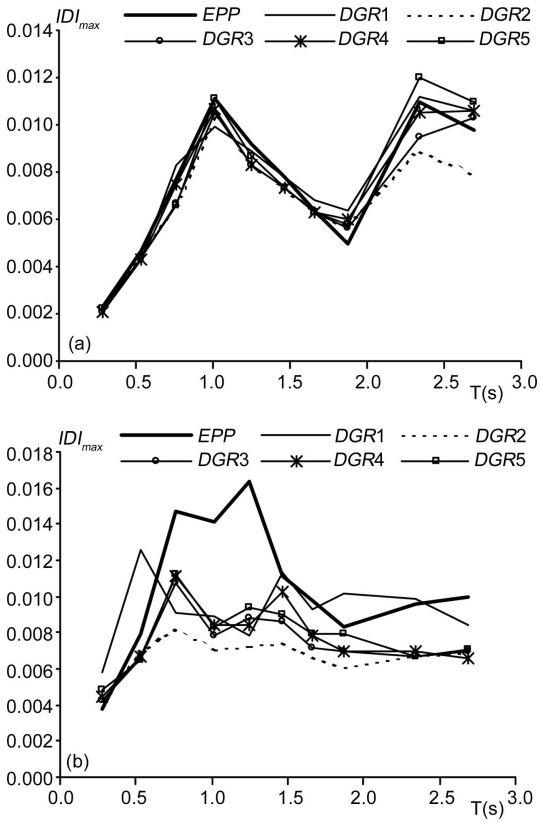

Figure 16. Maximum inter-storey drift demand, IDI_{max}, spectra. Influence of the hysteretic model. Stiffness distribution pattern *a*. Hachinoe *EW* (a) $\mu_{target} = 2$; (b) $\mu_{target} = 6$.

ductility demand and reflects the structural behaviour of structures designed more effectively according to the strong column-weak beam philosophy. The results obtained in this research in terms of median ratios between μ_{max} and μ_{target} are substantially close to those determined in [2]. However, it is important to underline that an appreciable variability can be identified when different motions are considered.

The influence of the hysteretic model on the top displacement demand (δ_{top}) is different from the effect on the inter-storey drift demand. In fact, in several cases it was possible to observe a reduction of δ_{top} even though a concentration of the drift was detected at storey level. Generally global demands, such as top displacement, are less affected by the strain hardening or strength deterioration during the unloading than the inter-storey drift demand.

Figures (16a), (16b), (17a) and (17b) illustrate the effects of the hysteretic model on the maximum inter-storey drift demand, IDI_{max}, for Hachinoe and Takatori record, respectively. Also in this case, the IDI_{max} demand spectra were obtained for target ductilities, μ_{target}, equal to 2 and 6. The IDI_{max} decreases with increasing strain hardening, especially

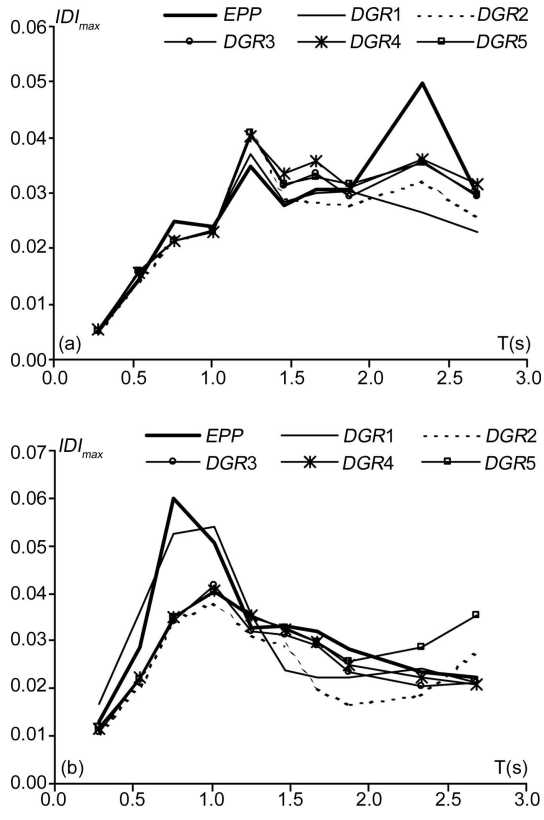

Figure 17. Maximum inter-storey drift demand, IDI_{max}, spectra. Influence of the hysteretic model. Stiffness distribution pattern *a*. Takatori (a) $\mu_{target} = 2$; (b) $\mu_{target} = 6$.

if target increases. For μ_{target} = 2, the IDI_{max} spectral curves are closer to each other in the whole period range and for motions recorded outside the near-field. However, it is possible to observe the largest drift demand of Takatori record, that is also amplified in absence of strain hardening.

Even though there is a substantial dispersion in the frequency content, amplitude, and duration of the analysed records, a median trend of the influence of the hysteretic model on the IDI_{max} can be identified. Figures (18a) and (18b) show the median IDI_{max} spectra for μ_{target} = 2 and μ_{target} = 6. The hysteretic model characterized by stiffness degradation during the unloading phase (*DGR*3 model) is subjected to drift demands larger than those observed in absence of such behaviour (*DGR*2 model). These differences depend significantly on the considered ground motion records and can reach a maximum of about 30%. On average, the abovementioned properties of the hysteretic models affect the local demands more than the global demands or those derived from the analyses of *SDOF* systems.

Structural performance can be influenced by the decrease of strength capacity during the reloading phase which also causes a reduction of the area enveloped by the hysteresis cycles. Such behaviour can be due to a progressive development of strength deterioration, which is quantified as a function of the hysteretic energy dissipation through inelastic cycles in the *DGR*5 model, or by pinching of the hysteresis loops of the *DGR*4 model. Both effects produce a reduction of the tangent stiffness during reloading, which implies a generally moderate increase of the drift demand, even though the degradation effects of the *DGR*4 and *DGR*5 models could be significantly marked.

However, the IDI_{max} demand is significantly affected by the strength deterioration when the ground motion contains several pulses of similar amplitude, so that the later pulses may contribute to further deterioration of strength. Near-fault records are thus less influenced by this effect, as they present only one or two strong pulses early in time histories. Moreover, the effects of strength deterioration or stiffness degradation are less important if the global displacement demand is concerned.

In Figures (19a) and (19b), where the median spectra of the parameter n_{IDImax}/H for μ_{target}=2 and 6

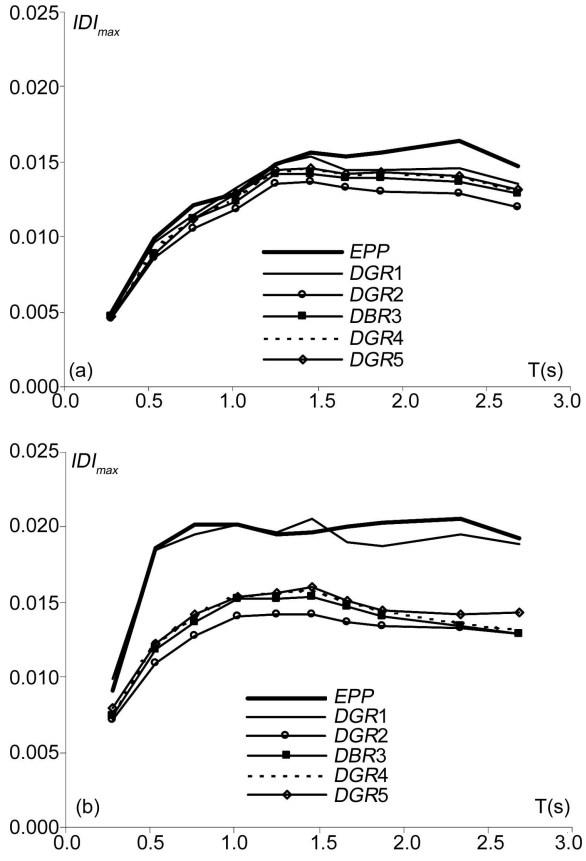

Figure 18. Median inter-storey drift demand, IDI_{max}, spectra. Influence of the hysteretic model. Stiffness distribution pattern *a*. (a) μ_{target} = 2; (b) μ_{target} = 6.

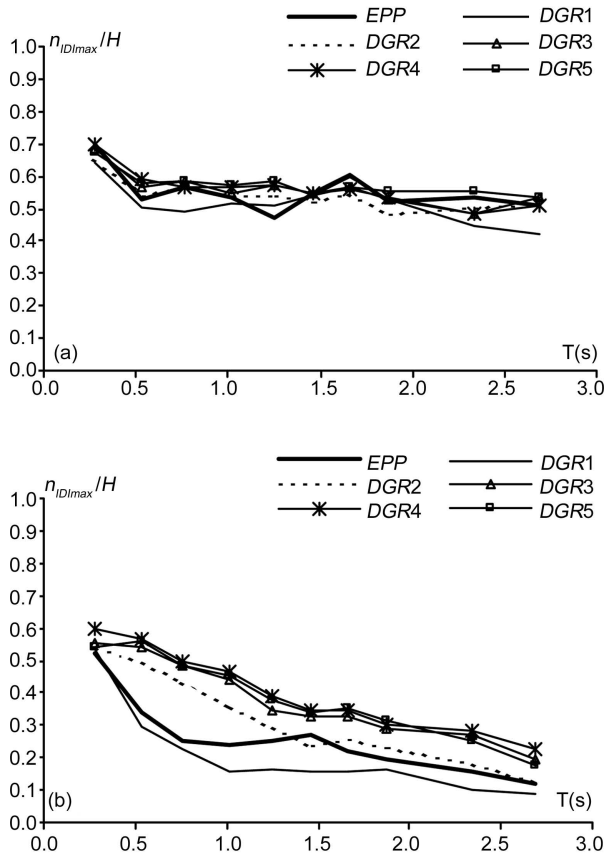

Figure 19. Median n_{IDImax}/H spectra. Influence of the hysteretic model. Stiffness distribution pattern *a*. (a) μ_{target} = 2 (b) μ_{target} = 6.

are shown, it is possible to observe a shift of the maximum inter-storey drift demands towards the bottom stories, which increases as the target ductility ratio increases. Such behaviour is more pronounced in the case of hysteretic models characterized by the absence of strain hardening (*EPP*, *DGR*1 models) or to a lesser degree, in the case of unloading stiffness degradation (*DGR*2 model).

Finally, the degrading models *DGR*3, *DGR*4, and *DGR*5 do not highlight significant differences in terms of ductility and drift demands and in the location where such maximum demands occur.

7. Conclusions

In the present study, an extensive parametric investigation was performed on different structures, subjected to recorded ground motions of different characteristics, in order to obtain a spectral representation of the most significant seismic deformation demand parameters in multi-storey frames. To this purpose, an adequate simplified shear-type model (*ESTM*), capable of giving a fairly accurate estimate of the seismic response of *MDOF* systems at global and local levels, was suitably defined and implemented. This kind of approach, even though more approximate than a complete nonlinear model of the frames, allowed to characterize adequately the influence of different target ductility ratios, stiffness distribution over the height and hysteretic models on the elastic and inelastic demands, in terms of top displacement and inter-storey drifts.

Based on this study, the following conclusions can be drawn:

- The drift distribution along the height of the frames, that simultaneously depends on both the earthquake ground motion and the structural characteristics is significantly influenced by the ductility ratio. Moreover, the inelastic inter-storey drift index (*IDI*) shows, on average, an amplification with respect to the elastic *IDI* in the short-period range, similarly to that obtained for the displacement demands for *SDOF* systems. As expected, the amplification of the inelastic *IDI* increases significantly with the increase of the ductility ratio.
- Another important influence on the drift demand is constituted by the stiffness distributions through the height of the multi-storey frames. The results obtained show that the stiffness distribution affects the inter-storey drift more than the top displacement, particularly in the inelastic range. Moreover, differences between the stiffness distribution patterns in terms of inelastic inter-storey drift demands are mainly due to the influence of the inelastic deflection shapes, which are significantly correlated with the stiffness distribution. The uniform stiffness distribution is confirmed to be inaccurate for seismic design, and seems to be inappropriate in evaluating the inelastic drift demand for real frames. Finally, for the stiffness distribution patterns *a* and *b*, reliable values of the coefficient of distortion *COD* were suggested, which relates maximum inter-storey drift to the average drift along the height of the frame. The assessment of such parameter is necessary in the preliminary design in order to evaluate the maximum inter-storey drift demand to be compared iteratively with the maximum drift supplied by the structure.
- The choice of a given type of hysteretic model, which represent the approximate degree of local inelastic deformation demand, affects the response to ground motion significantly. This is particularly evident in the absence of strain hardening, and detectable in both the *EPP* and *DGR*1 hysteretic models, which causes a strong local concentration of drift and ductility demands. However, it is important to underline that an appreciable variability can be recognized when different motions are considered. Generally global demands, such as top displacement, are less affected by the strain hardening or strength deterioration during the unloading than the inter-storey drift demand. The inter-storey drift demand is also affected by the decrease of strength capacity during the reloading phase, which also causes a reduction of the area enveloped by the hysteresis cycles. This behaviour, principally taken into account by the *DGR*4 and *DGR*5 models, is significant for long duration ground motions, particularly if the time histories include several pulses of similar amplitude. Finally, the degrading models *DGR*3, *DGR*4, and *DGR*5 do not show noteworthy differences in terms of ductility and drift demands.

Acknowledgments

This work was supported by the Italian Ministry of Education, University and Research (*MIUR*). We wish to express our gratitude to Dr. Paolo Bazzurro, Prof. Paolo Maria Mariano, and Dr. Silvia Bruno for their valuable suggestions and comments. We also thank the anonymous reviewers for their constructive remarks that contributed to improve the manuscript.

References

1. Uang, C.M. and Bertero, V.V. (1990). "Evaluation of Seismic Energy in Structures", *Earthquake Engineering and Structural Dynamics*, **19**, 77-90.

2. Nassar, A.A. and Krawinkler, H. (1991). "Seismic Demands for SDOF and MDOF Systems", John A. Blume Earthquake Engineering Center Report No. 95, Department of Civil Engineering, Stanford University.

3. Fajfar, P. and Vidic, T. (1994). "Consistent Inelastic Design Spectra: Hysteretic and Input Energy", *Earthquake Engineering and Structural Dynamics*, **23**, 523-532.

4. Decanini, L. and Mollaioli, F. (1998). "Formulation of Elastic Earthquake Input Energy Spectra", *Earthquake Engineering and Structural Dynamics*, **27**, 1503-1522.

5. Decanini, L. and Mollaioli, F. (2001). "An Energy-Based Methodology for the Assessment of Seismic Demand", S*oil Dynamics and Earthquake Engineering*, **21**, 113-137.

6. Teran-Gilmore, A. (1998). "A Parametric Approach to Performance-Based Numerical Seismic Design", *Earthquake Spectra*, **14**(3), 501-520.

7. Krawinkler, H., Medina, R., Miranda, M., and Ayoub, A. (1999). "Seismic Demands for Performance-Based Design", *Proc. of the U.S.-Japan Workshop on Performance-Based Earthquake Engineering Methodology for Reinforced Concrete Building Structures*, PEER Report 1999/10, Maui, Hawaii.

8. Leelataviwat, S., Goel, S.C., and Stojadinovic, B. (1999). "Toward Performance-Based Seismic Design of Structures", *Earthquake Spectra*, **15**(3), 435-461.

9. Bommer, J.J. and Elnashai, A.S. (1999). "Displacement Spectra for Seismic Design", *J. of Earthquake Engineering*, Imperial College Press, **3**(1), 1-32.

10. Miranda, E. (2000). "Inelastic Displacement Ratios for Structures on Firm Sites", *ASCE J. of Structural Engineering*, **126**(10), 1150-1159.

11. Miranda, E. (2001). "Estimation of Inelastic Deformation Demands of SDOF Systems", *ASCE J. of Structural Engineering*, **127**(9), 1005-1012.

12. Krawinkler, H., Medina, R., and Alavi, B. (2003). "Seismic Drift and Ductility Demands and Their Dependence on Ground Motions", *Engineering Structures*, **25**, 637-653.

13. Bertero, R.D. and Bertero, V.V. (1992). "Tall Reinforced Concrete Buildings: Conceptual Earthquake-Resistant Design Methodology", Report No. UCB/EERC-92/16, University of California, Berkeley.

14. Iwan, W.D. (1997). "Drift Spectrum: Measure of Demand for Earthquake Ground Motions", *ASCE J. of Structural Engineering*, **123**(4), 397-404.

15. Miranda, E. (1999). "Approximate Seismic Lateral Deformation Demands in Multistory Buildings", *ASCE J. of Structural Engineering*, **125**(4), 417-425.

16. Iwan, W.D., Huang, C.T., and Guyader, A.C. (2000). "Important Features of the Response of Inelastic Structures to Near-Field Ground Motion", *Proc. of the 12th World Conf. on Earthquake Engineering*, Auckland, New Zealand.

17. Krawinkler, H. and Seneviratna, G.D.P.K. (1998). "Pros and Cons of a Pushover Analysis of Seismic Performance Evaluation", *Engineering Structures*, **20**(4-6), 452-464.

18. Chintanapakdee, C. and Chopra, A.K. (2003). "Evaluation of Modal Pushover Analysis Using Generic Frames", *Earthquake Engineering and Structural Dynamics*, **32**, 417-442.

19. Vamvatsikos, D. and Cornell, C.A. (2002). "Incremental Dynamic Analysis", *Earthquake Engineering and Structural Dynamics*, **31**, 491-514.

20. Decanini, L., Mollaioli, F., and Mura, A. (2002). Shear-Beam Model for the Prediction of the Response of MDOF Systems Subjected to Severe Earthquake Ground Shaking", *12th European Conference on Earthquake Engineering*, Elsevier Science Ltd., London.

21. Decanini, L., Mollaioli, F., and Mura, A. (2004).

"Simplified Shear-Type Model for the Evaluation of the Influence of Ductility and Stiffness Distribution Patterns on Multi-Story Structures", XI Italian National Conference *L'ingegneria Sismica in Italia*, Genova, Italy, Padova, SGE, p. 215 e CD ref. D1-01.

22. Watson, S. (1989). "Design of Reinforced Concrete Frames of Limited Ductility", Research Report 89/4, Department of Civil Engineering, University of Canterbury, Christchurch, New-Zealand.

23. Park, R. and Paulay, T. (1975). "Reinforced Concrete Structures", John Wiley and Sons, New York.

24. Mazza, F. and Vulcano, A. "Effects of Near-Fault Ground Motions on the Response of RC Framed Structures Designed According to Eurocode 8", *12th European Conference on Earthquake Engineering*, Elsevier Science Ltd, London.

25. EC8 (Eurocode 8), "European Standard Design of Structures for Earthquake Resistance", Pr DRAFT No. 3.

26. Singhal, A. and Kiremidjian, A. (1997). "A Method for Earthquake Motion-Damage Relationships with Application to Reinforced Concrete Frames", Technical Report NCEER-97-0008, Buffalo.

27. Gupta, A. and Krawinkler, H. (2000). "Estimation of Seismic Drift Demands for Frame Structures", *Earthquake Engineering and Structural Dynamics*, **29**,1287-1305.

28. Mura, A. (2003). "Sulla Valutazione Del Potenziale di Danno in Termini di Spostamenti e di Energia sui Sistemi a più Gradi di Libertà Soggetti ad Eccitazione Sismica", Ph.D. Dissertation Thesis, Department of Structural and Geotechnical Engineering, University of Rome "La Sapienza", (in Italian).

29. Seneviratna, G.D.P.K., Krawinkler, H. (1997). "Evaluation of Inelastic MDOF Effects for Seismic Design", John A. Blume Earthquake Engineering Center Report No.120, Department of Civil Engineering, Stanford University.

30. Kunnath, S.K., Reinhorn, A.M., and Lobo, R.F. (1992). "IDARC 3.0: A Program for the Inelastic Damage Analysis of Reinforced Concrete Structures", Technical Report NCEER-92-0022 State University of New York at Buffalo.

31. Clough, R.W. and Johnston, S.B. (1966). "Effect of Stiffness Degradation on Earthquake Ductility Requirements", *Proc. of Japan Earthquake Engineering Symposium*, Tokyo, Japan, 227-332.

32. Takeda, T., Sozen, M.A., and Nielsen, N.N. (1970). "Reinforced Concrete Response to Simulated Earthquakes", *ASCE Journal of the Structural Division*, **96**(ST12).

33. Housner, G.W. (1952). "Spectrum Intensities of Strong Motion Earthquakes", *Proc. of the Symposium of Earthquake and Blast Effects on Structures*, EERI, Los Angeles, California, 21-36.

34. Hwang, H. and Jaw, J. (1990). "Statistical Evaluation of Deflection Amplification Factors for Reinforced Concrete Frames", *Proc. of the Fourth U.S. National Conference on Earthquake Engineering*, **2**, 937-944.